Detection of caspase-3 and caspase-7 activation

Cell lines with dox-controlled del32–71 GH expression were seeded at a density of 2.5×10^4 cells/150 μL of culture medium into 96-well culture plates in the presence or absence of 100 ng/mL dox. Six wells for each cell line were visualized using an Image-iT LIVE Red Caspase-3 and -7 Detection Kit (Molecular Probes; Invitrogen) 24 hours after induction. Twenty pictures for each cell line were taken under a fluorescence microscope with ×200 magnification. At least 3800 cells for each cell line were counted, and cells producing luminescence above a certain threshold intensity were judged as caspase-positive using WinROOF (Mitani Corp., Tokyo, Japan). The threshold was kept constant in all cell lines.

Image analysis and statistics

Expression levels of ER stress response genes were statistically evaluated by the Student t test. The ratio of caspase-3– and caspase-7–positive cells to total cells under a fluorescence microscope and the ratio of vacuole area to cytosol area under an electron microscope were evaluated using WinROOF and statistically evaluated by a Student t test. The ratio of apoptotic cells to surviving cells after overexpression of XBP1(S) was analyzed by the χ^2 test.

Results

Concentrations of wild-type GH secreted in culture media decreased with induction of del32–71 GH

For the purpose of evaluating ER stress caused by del32–71 GH, GH4C1 cell lines with dox-controlled del32–71 GH expression, in which wild-type GH was stably expressed and del32–71 GH expression was induced by removing dox from the culture medium, were established. In the classic stable cell lines established by constructs using a cytomegalovirus promoter, we observed preferential growth of cells resistant to del32–71 GH–induced ER stress, and ER stress responses were presumably diluted after successive culturing. Establishment of these dox-controlled cell lines enabled us to suppress del32–71 GH expression by adding dox continuously into the culture media, thereby minimizing this selection bias. In addition, these cell lines enabled us to evaluate del32–71 GH–induced ER stress by comparing cells in the presence or absence of dox-mediated induction under the same genetic background.

First, concentrations of wild-type GH in culture media were evaluated by IRMA for all 23 dox-controlled cell lines with or without del32–71 GH induction. In 20 of the 23 cell lines, wild-type GH concentrations in the media decreased by 18.8% to 62.6% with del32–71 GH induction, suggesting that the expression of del32–71 GH caused a dominant negative effect on wild-type GH secretion in these 20 cell lines (Figure 1A). Median wild-type GH concentrations among the 23 cell lines were 31.68 ng/mL (range, 7.78–84.00 ng/mL) and 18.18 ng/mL (range, 5.50–66.33 ng/mL), without and with del32–71 GH induction, respectively.

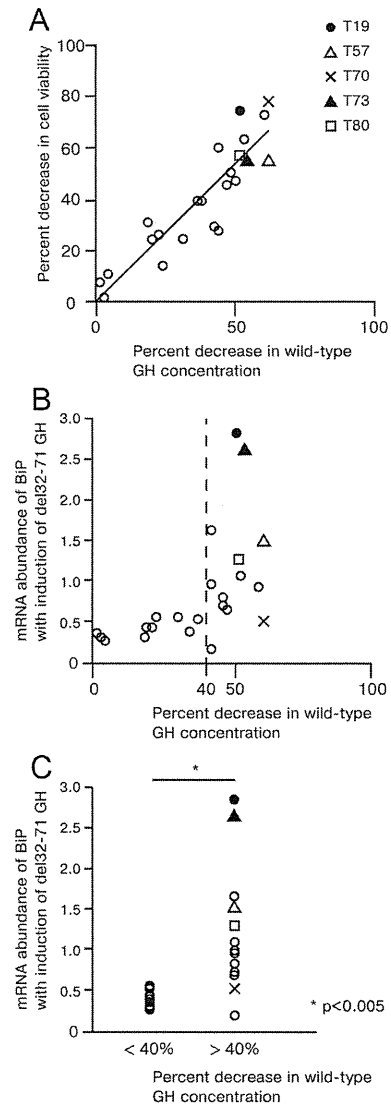

Figure 1. Demonstration of the dominant negative effect of del32–71 GH on wild-type GH secretion using cell lines with dox-controlled del32–71 GH expression. A and B, 23 cell lines with dox-controlled del32–71 GH expression were seeded at a density of 2.5×10^4 cells/150 μL in a 96-well culture plate in the presence or absence of 100 ng/mL dox. At 48 hours later, the concentrations of wild-type GH in the medium were measured by IRMA. Then, a 1/10 volume of CCK-8 reagent was added to the culture medium, and absorbance at 450 nm was measured 4 hours later using a multiplate reader. The relationships between the decrease in the wild-type GH concentration (−dox/+dox, horizontal axis) and the following factors (vertical axis) are shown: decrease in cell viability (−dox/+dox) (A) and mRNA abundance of BiP (−dox) by qRT-PCR normalized to β-actin (B). The dotted line indicates a 40% decrease in wild-type GH concentration. Each factor was measured 3 times, and means are shown. C, A difference in BiP transcripts between cells with decreases in wild-type GH secretion by less than 40% and cells with decreases by more than 40%. ●, T19 cell line; △, T57 cell line; ×, T70 cell line; ▲, T73 cell line; □, T80 cell line; ○, other dox-controlled cell lines.

Dominant negative effect was positively correlated with cell viabilities

Next, cell viabilities of the 23 dox-controlled cell lines were evaluated using CCK-8 reagent with or without induction. In the 20 clones in which the wild-type GH concentration in the culture medium decreased, cell viabilities also decreased by 14.3% to 78.0% after del32–71 GH induction. In addition, the wild-type GH concentrations in the culture medium were positively correlated with cell viability in these 23 cell lines, suggesting the association between the dominant negative effect of del32–71 GH and cell viability (Figure 1A).

mRNA abundance of ER stress markers was significantly higher in cells with large decreases in wild-type GH secretions than in cells with small decreases

The association between the dominant negative effect and cell viability led us to hypothesize that these 2 factors were associated with del32–71 GH–induced ER stress. To test this hypothesis, we evaluated a relationship between the wild-type GH concentrations (described above) and abundance of *BiP* transcripts with del32–71 GH induction in the 23 cell lines (Figure 1B). BiP was used as an ER stress marker because it is a well-known ER chaperone that binds to the hydrophobic region of unfolded proteins (see *Materials and Methods*) (12). A significant difference existed in *BiP* transcripts (normalized to β-actin) between cells with decreases in wild-type GH concentrations by less than 40% and those with decreases by more than 40% (Figure 1, B and C). Abundance of *XBP1(S)* transcripts, another ER stress response marker that enhances the transcription of ERAD components, was also evaluated with similar results (data not shown).

Five cell lines with dox-controlled del32–71 GH expression were selected as the cellular model

Thus, T19, T57, T70, T73, and T80 cell lines were chosen as the cellular model; wild-type GH secretion was severely decreased by the induction of del32–71 GH in these 5 cell lines, and the involvement of ER stress appeared to be large in T19 and T73 cells, medium in T57 and T80 cells, and small in T70 cells, as measured by *BiP* and *XBP1(S)* mRNA expression (Figure 1, A–C). We intentionally chose these 5 cell lines because *BiP* and *XBP1(S)* transcripts were variable even when wild-type GH secretion was decreased by more than 40% (Figure 1C).

qRT-PCR was performed to evaluate the expression of wild-type and del32–71 GH in these 5 cell lines. The expression of del32–71 GH increased 9.71- to 54.4-fold with the induction of del32–71 GH (Figure 2A), and, as a result, the abundance of del32–71 GH transcripts was compa-

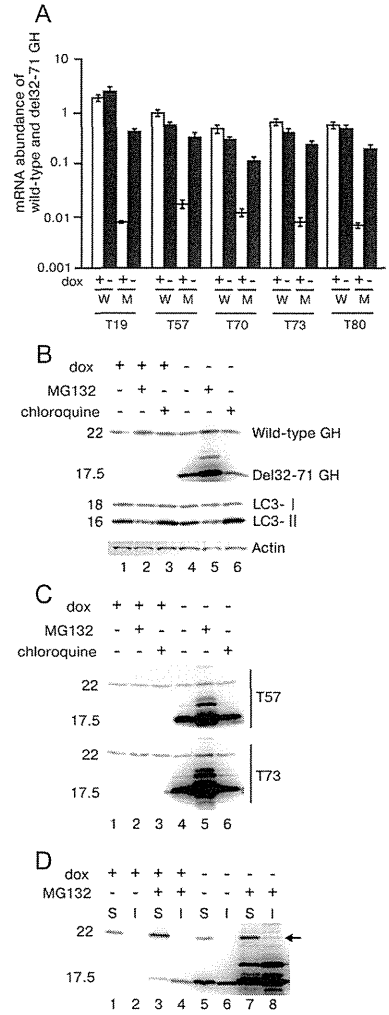

Figure 2. Evaluation of wild-type and del32–71 GH expression using the 5 cell lines with dox-controlled del32–71 GH expression. A, mRNA abundance of wild-type and del32–71 GH was evaluated by qRT-PCR using primers located within exon 3 for wild-type GH and spanning exon 2 and exon 4 for del32–71 GH; relative expression was calculated by normalization to β-actin expression. The means and SDs for 3 independent experiments were measured. W, wild-type GH; M, del32–71 GH. B, Immunoblotting of T19 cell lysate. Whole-cell lysates (30 μg/lane) were separated by SDS-PAGE, and immunoblotting was performed using antibodies for GH, LC3, and actin. Lane 1,100 ng/mL dox; lane 2, 10 μM MG132 with dox; lane 3, 50 μg/mL chloroquine with dox; lane 4, without dox; lane 5, 10 μM MG132 without dox; lane 6, 50 μg/mL chloroquine without dox. Similar results were obtained in 3 independent experiments. C, Immunoblotting of T57 and T73 cell lysates using antibodies for GH. Lane 1, 100 ng/mL dox; lane 2, 10 μM MG132 with dox; lane 3, 50 μg/mL chloroquine with dox; lane 4, without dox; lane 5, 10 μM MG132 without dox; lane 6, 50 μg/mL chloroquine without dox. D, Immunoblotting of soluble and insoluble fractions of T19 cell lysate using antibodies for GH. S, soluble fraction; I, insoluble fraction. Lanes 1 and 2, 100 ng/mL dox; lanes 3 and 4, 10 μM MG132 with dox; lanes 5 and 6, without dox; lanes 7 and 8, 10 μM MG132 without dox. Arrow indicates 22-kDa wild-type GH signal in insoluble fraction. The 17.5-kDa signals were detected even without the induction of del32–71 GH after MG132 treatment (lanes 3 and 4), indicating that leaky expression of del32–71 GH was observed.

rable with that of wild-type GH transcripts after the induction (Table 1). These data suggested that these 5 cell lines were appropriate cellular models for patients with the *GH1* gene splice site mutations; the transcript ratio of wild-type to del32–71 GH is theoretically 1:1.

del32–71 GH was degraded in a proteasome-dependent manner

Figure 2B shows the result of immunoblotting in T19 cell lysates. The removal of dox from the culture medium induced the expression of del32–71 GH, and treatment with the proteasome inhibitor MG132 markedly increased the 17.5-kDa signal, as reported previously (Figure 2B, lanes 4 and 5) (21, 22). The increase in the 17.5-kDa del32–71 GH signal was not demonstrated by chloroquine treatment, which disturbs lysosomal degradation by elevating the pH in the lysosome (Figure 2B, lanes 4–6). LC3-I is converted to LC3-II through the formation of autophagosomes, and LC3-II localizes in the autophagosomal membrane. Autophagosomes bind to lysosomes, and thus lysosomal inhibition is known to cause accumulation of LC3-II (23). Therefore, the increased LC3-II signal indicated that chloroquine treatment disturbed lysosomal function. These data suggested that del32–71 GH was a target of proteasome-dependent degradation, which is consistent with previous data demonstrating that del32–71 GH was localized within the ER (5, 6) and degraded via ERAD (21, 22). Note that MG132 is specific for ERAD. We confirmed the same pattern of immunoblotting in T57 and T73 cells (Figure 2C).

Coaggregation of wild-type and del32–71 GH was unlikely to be the major cause of the dominant negative effect

For the purpose of evaluating wild-type and del32–71 GH protein interactions, we investigated whether del32–71 GH coaggregated with wild-type GH. Unfolded proteins tend to aggregate, and such aggregated mutant proteins can involve normal proteins expressed from the other wild-type allele, causing a dominant negative effect (24). Previous studies have shown that aggregated mutant proteins have low solubility in 1% Triton X-100 (14, 22, 25). Thus, in the present study, T19 cells were lysed in 1% Triton X-100 in the presence or absence of del32–71 GH induction, and soluble/insoluble fractions were separately isolated for evaluation of each fraction by immunoblotting. A small amount (4.5%) of wild-type GH was detected in the insoluble fraction with the induction of del32–71 GH after MG132 treatment, whereas about half of del32–71 GH was detected in the insoluble fraction (Figure 2D, lanes 5–8). These data suggested that coaggregation of wild-type and del32–71 GH could exist but was unlikely to be the major cause of the dominant negative effect.

Table 1. mRNA Abundance Ratios for Wild-Type to del32–71 GH in the 5 dox-Controlled Cell Lines With and Without Induction of del32–71 GH

	mRNA Abundance Ratio of Wild-Type to del32–71 GH				
	T19	T57	T70	T73	T80
+ dox	229	51.4	39.0	79.6	85.8
− dox	5.74	1.71	2.60	1.69	2.33

Data represent ratios of the relative expression of wild-type to del32–71 GH (±100 ng/mL dox) evaluated by qRT-PCR after normalization to β-actin expression. Means of 3 independent experiments are shown.

del32–71 GH activated ER stress responses via the PERK, ATF6, and IRE1 pathways

The proteasome-dependent del32–71 GH degradation and the little involvement of wild-type GH in del32–71 GH aggregate led us to evaluate ER stress responses in the 5 cell lines with dox-controlled del32–71 GH expression. Three major pathways, the PERK, ATF6, and IRE1 pathways, are known to act as ER stress responses in mammalian cells as described in the Introduction. PERK, ATF6, and IRE1 are sensor molecules located in the membrane of the ER and are activated by the accumulation of unfolded proteins in the ER. These activated sensor molecules transduce signals to suppress the translation of proteins, enhance the folding capacity of ER chaperones, and promote the degrading function of ERAD machinery in the respective pathways (12). For each pathway, the following target genes were chosen: *GADD34* and *CHOP* for the PERK pathway, *BiP* and *GRP94* for the ATF6 pathway, and *XBP1* for the IRE1 pathway.

In T19, T57, T73, and T80 cell lines, the abundance of the target gene transcripts significantly increased after del32–71 GH induction, suggesting that the PERK and ATF6 pathways were activated by del32–71 GH induction in these 4 cell lines (Figure 3, A–D). In the T70 cell line, levels of these 4 target genes were significantly elevated, whereas the degree of activation was small compared with that of the other 4 cell lines (Figure 3, A–D).

In the same 4 cell lines, XBP1 was activated. XBP1 is a nuclear transcription factor that can be activated by IRE1, enhancing the transcription of ERAD components. IRE1 converts inactive *XBP1* [*XBP1(U)*] mRNA into active *XBP1* [*XBP1(S)*] mRNA by splicing out 26 bp, located between the DNA-binding domain and DNA-activating domain (12, 26, 27). The activation of *XBP1* can be detected by RT-PCR using primers that surround these 26 bp, yielding 140- and 114-bp PCR products corresponding to *XBP1(U)* and *XBP1(S)*, respectively. The higher the

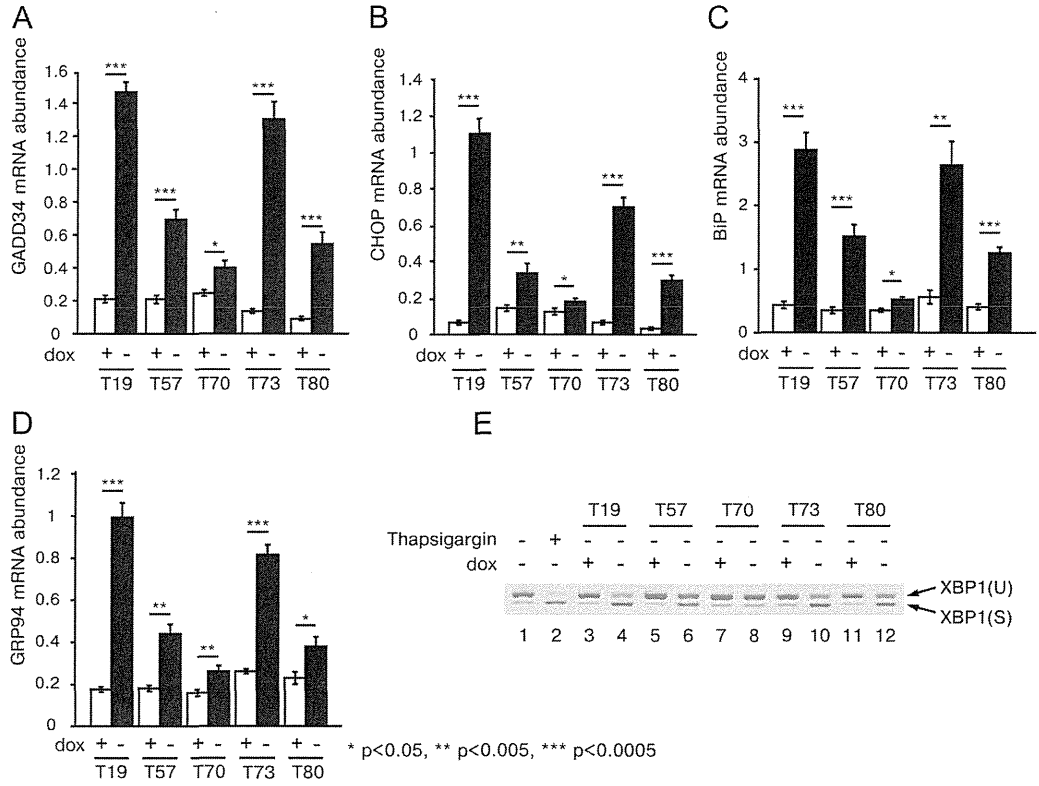

Figure 3. del32–71 GH induction activated ER stress responses via the PERK, ATF6, and IRE1 pathways. A–D, expression of GADD34 (A), CHOP (B), BiP (C), and GRP94 (D) transcripts in T19, T57, T70, T73, and T80 cell lines in the presence or absence of 100 ng/mL dox, as measured by qRT-PCR. Means and SDs from 3 independent experiments are shown, with relative abundance calculated by normalization to β-actin expression. Data were statistically evaluated using the Student *t* test. E, Splicing of XBP1 mRNA. mRNA from T19, T57, T70, T73, and T80 cell lines (±100 ng/mL dox) was converted to cDNA, and RT-PCR was performed. Samples were applied to a 3.5% agarose gel. XBP1(U), unspliced XBP1; XBP1(S), spliced XBP1; lane 1, untreated GH4C1 cells; lane 2, thapsigargin-treated GH4C1 cells; lanes 3 and 4, T19; lanes 5 and 6, T57; lanes 7 and 8, T70; lanes 9 and 10, T73; and lanes 11 and 12, T80. Similar results were obtained in 3 independent experiments for all 5 cell lines.

ratio of *XBP1(S)* to *XBP1(U)*, the more XBP1 is considered to be activated. As shown in Figure 3E, XBP1 was activated in T19, T57, T73, and T80 cell lines, suggesting that del32–71 GH induction activated the IRE1 pathway (Figure 3E, lanes 3–6 and 9–12). In the T70 cell line, XBP1 was not activated (Figure 3E, lanes 7 and 8).

In summary, all of the 3 major ER stress response pathways were demonstrated to be activated by the induction of del32–71 GH in T19, T57, T73, and T80 cell lines.

Dox treatment/removal could have some effects on cell physiology independent of del32–71 GH expression. Therefore, using the parental cell line expressing only wild-type GH, we evaluated wild-type GH concentrations in the media, cell viability, and ER stress responses. No significant differences were found after dox treatment/removal in this parental cell line, suggesting that dox administration itself did not have any significant effects on cell physiology (Supplemental Figure 1, A–D).

Marked proliferation and enlargement of the ER was observed by the induction of del32–71 GH under electron microscopy (EM)

To investigate the impact of del32–71 GH on cellular morphology, EM images of T80 cells were evaluated in the presence or absence of del32–71 GH induction. In high-power fields, marked proliferation and enlargement of the ER were demonstrated in some T80 cells after del32–71 GH induction (Figure 4, A–C). ER stress responses are known to stimulate ER synthesis to increase the folding capacity of ER chaperones, enhance the function of ERAD machinery, and dilute the unfolded protein load (28). Thus, these EM images were consistent with the activation of ER stress responses after del32–71 GH induction.

In low-power fields, many vacuoles appeared within the cytosol after the induction of del32–71 GH expression (Figure 4D). The number of vacuoles varied in T80 cells, ie, vacuoles did not exist in all induced T80 cells. However, ratios of vacuole area to cytosol area were significantly increased after induction (Figure 4E). Although autophagy is another mechanism through which unfolded

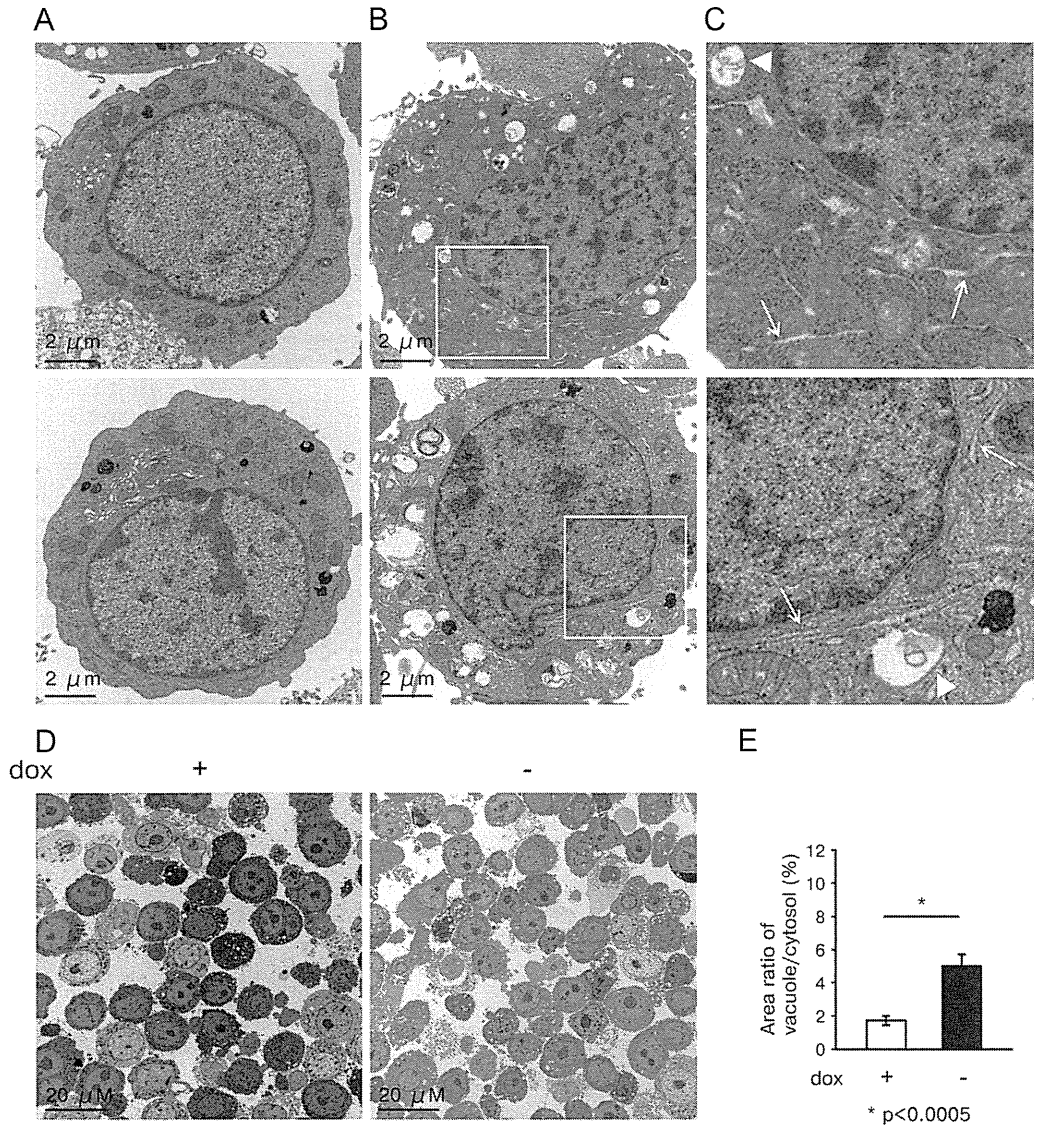

Figure 4. EM images of the T80 cell line. A, High-power fields, in the presence of 100 ng/mL dox. B, High-power fields, in the absence of dox. C, Enlarged pictures of the indicated areas in B. Marked accumulation of the rough ER (arrow) and vacuoles (arrowhead) was observed. D, Low-power fields, in the presence or absence of dox. The number of vacuoles was increased by del32–71 GH induction. E, Ratio of vacuole area to cytosol area was calculated using WinROOF. Means and SEMs for 29 and 36 EM images, without and with del32–71 GH induction, respectively, were statistically evaluated by the Student *t* test.

protein can be degraded and is known to be activated by ER stress (23), these vacuoles were not thought to be LC3-dependent autophagosomes; LC3-II translocation was not shown by either immunoblotting (Figure 2B, lanes 1 and 4) or immunofluorescence (data not shown).

Induction of del32–71 GH caused apoptosis

Next, we evaluated whether the induction of del32–71 GH caused apoptosis in these cells. DNA samples from T19 cells were extracted every 12 hours after del32–71 GH induction and subjected to electrophoresis. Induction of del32–71 GH for 12 hours caused DNA fragmentation in T19 cells, suggesting the occurrence of apoptosis (Figure 5A).

del32–71 GH induction also caused activation of caspase-3 and -7, an early sign of apoptosis, in T19, T57, T73, and T80 cells (Figure 5, B and C). Caspases are well-known proapoptotic components, and caspase-3 and -7 have been reported to be involved in ER stress–induced cell death (29). With use of the image-analyzing software WinROOF, caspase-positive (apoptotic) cells and Hoechst33428-positive (surviving) cells were counted (see *Materials and Methods*). Ratios of caspase-positive cells to total cells were significantly increased with the induction

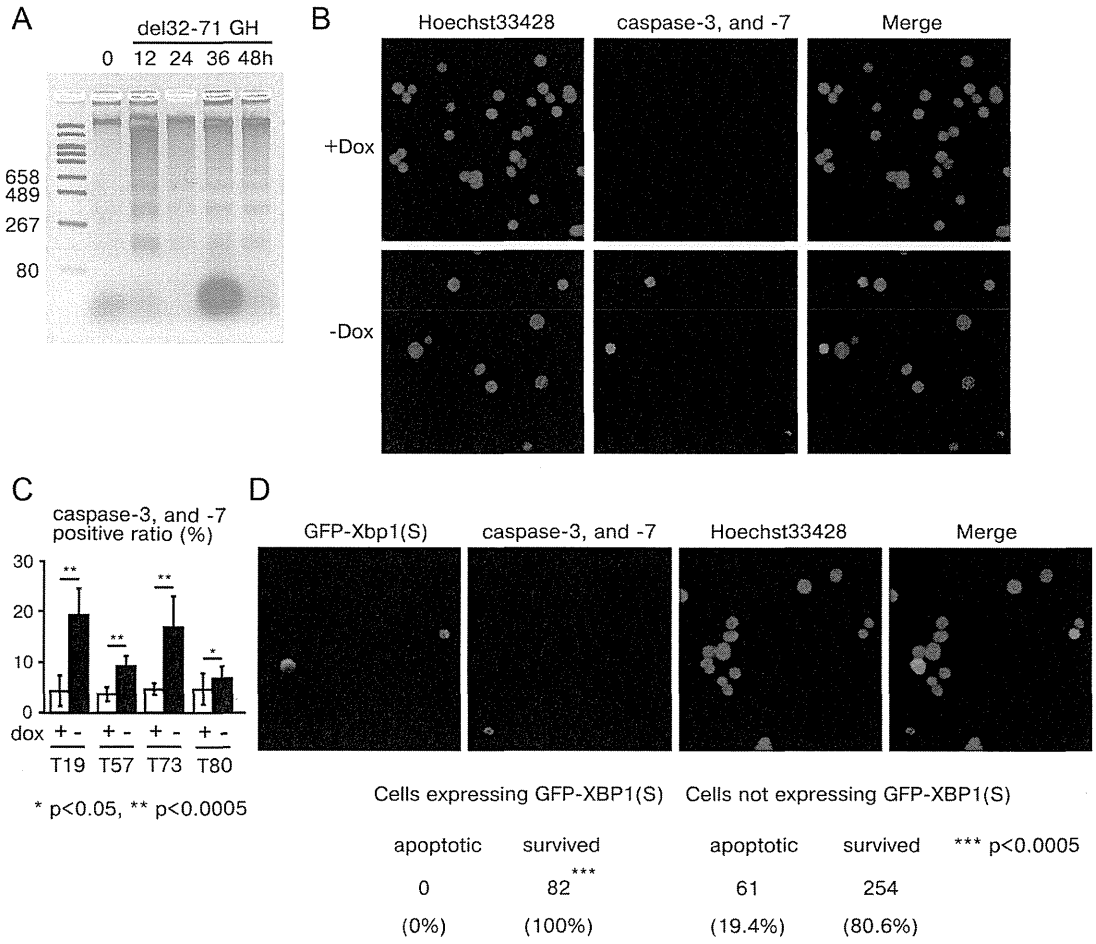

Figure 5. del32–71 GH induction caused ER stress, leading to apoptosis. A, DNA fragmentation caused by the induction of del32–71 GH. T19 cells were incubated without dox for the indicated times and evaluated for DNA fragmentation. Chromosomal DNA was extracted, separated on a 2% agarose gel and then visualized by staining with GelRed. B, Activation of caspase-3 and -7 by the induction of del32–71 GH. The expression of del32–71 GH was induced in T19, T57, T73, and T80 cell lines, and the activation of caspase-3 and -7 was evaluated 24 hours later using the Image-iT LIVE Red Caspase-3 and -7 Detection Kit. Hoechst33428-positive cells indicate surviving cells, and rhodamine-positive cells indicate apoptotic cells. C, The ratio of rhodamine-positive cells to total cells in B was calculated by WinROOF. Means and SDs for 10 independent experiments were measured, and statistical evaluations were conducted using the Student *t* test. D, GFP-XBP1(S) was overexpressed in T73 cells, and the expression of del32–71 GH was induced 24 hours later. After an additional 24 hours, activation of caspase-3 and caspase-7 was evaluated, and cells were photographed under a fluorescence microscope. The numbers of apoptotic and surviving cells were counted (bottom). The data were statistically evaluated using the χ^2 test.

of del32–71 GH in these 4 cell lines, suggesting that del32–71 GH–induced apoptosis was associated with ER stress (Figure 5C).

Overexpression of XBP1(S) rescued del32–71 GH–mediated apoptosis

To confirm a causal relationship between ER stress and apoptosis, we finally examined whether the introduction of XBP1(S), a nuclear transcription factor that enhances the transcription of ERAD components, could rescue del32–71 GH–induced apoptosis. In a previous study, overexpression of XBP1(S) was reported to rescue thapsigargin-induced apoptosis (27). Thus, T73 cells were transfected with GFP-XBP1(S) followed by induction of del32–71 GH expression and evaluation for the activation of caspase-3 or -7. The overexpression of XBP1(S) completely reversed the activation of caspase-3 and -7 (Figure 5D), suggesting that the induction of del32–71 GH caused ER stress, which subsequently triggered apoptosis.

Discussion

Our hypothesis for the molecular mechanism of the dominant negative effect, together with data reported in other studies, is shown in Figure 6. The major finding of our study was that the induction of del32–71 GH activated ER stress responses, causing apoptosis in our pituitary-derived cell lines.

Several studies have investigated the molecular mechanisms mediating the dominant negative effect of

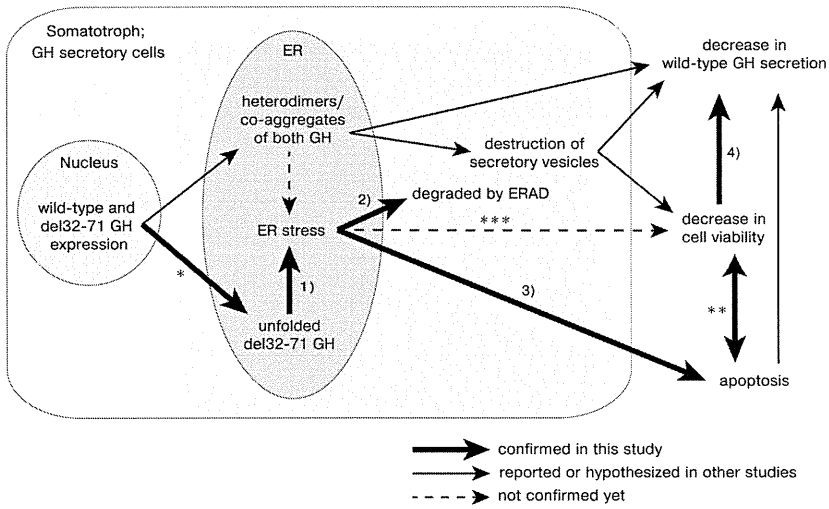

Figure 6. A model for the molecular mechanism of the dominant negative effect. Thick arrows represent data confirmed in the current study, arrows represent data reported in other studies, and dashed arrows represent data not confirmed yet. In this study, we demonstrated that (1) ER-localized del32–71 GH caused ER stress, (2) del32–71 GH was degraded by a proteasome-dependent manner via ERAD, (3) ER stress caused by del32–71 GH triggered apoptosis, and (4) the decrease in cell viability and wild-type GH secretion were associated. *, We confirmed localization of del32–71 GH in the ER by an immunofluorescence study (data not shown). **, It is difficult to evaluate a causal association between the decrease in cell viability and apoptosis; the former can be a result of the latter and vice versa. ***, A causal relationship between ER stress and decrease in cell viability is speculated but not proven; we did not evaluate cell viability and wild-type GH secretion in the cells that are rescued by overexpression of XBP1(S).

del32–71 GH. Hayashi et al (30) showed that cotransfection of wild-type and del32–71 GH leads to a decrease in wild-type GH secretion using pituitary-derived cell lines. Iliev et al (31), Lee et al (32), and Salemi et al (33) demonstrated that transfection of neuroendocrine cells with wild-type GH and del32–71 GH suppresses the accumulation and secretion of wild-type GH. McGuinness et al (7) demonstrated a decrease in the proliferation rate and destruction of secretory vesicles using GC cells stably expressing del32–71 GH, and Kannenberg et al (22) established double-transfected stable GH4C1 cell lines using wild-type and del32–71 GH constructs, demonstrating that aggregated wild-type and del32–71 GH were degraded by the proteasome. These previously published data suggested that the dominant negative effect of del32–71 GH may be caused by protein interactions, such as coaggregates of wild-type and del32–71 GH.

Theoretically, del32–71 GH exerts a dominant negative effect on the production and secretion of wild-type GH in 3 steps: (1) mRNA levels, reducing wild-type GH mRNA by mechanisms such as rapid degradation; (2) protein levels, promoting degradation of wild-type GH with degradation of del32–71 GH as a result of heterodimers or aggregates; and (3) cellular characteristics, including a decrease in overall cell viability and apoptosis, for example, that caused by ER stress. In our study, involvement of the first step in the dominant negative effect was unlikely because the abundance of wild-type GH transcripts did not change with del32–71 GH induction (Figure 2A). Hamid et al (34) reported that both the amount of del32–71 or wild-type GH transcripts and the ratio of del32–71 to wild-type GH transcripts correlated with differences in height SD scores in patients with the same *GH1* gene splice site mutation (34). These data suggested that some unknown function of del32–71 GH, which acts to suppress the transcription or promote the degradation of wild-type GH mRNA, may exist.

Next, we speculated that the involvement of the second step, protein interactions, in the dominant negative effect was unlikely, because little wild-type GH was detected in the insoluble fraction with the induction of del32–71 GH after MG132 treatment (Figure 2D). However, previous reports have demonstrated that wild-type and del32–71 GH coaggregate (7, 22). Heterodimers and the involvement of wild-type GH in del32–71 GH aggregates are both widely accepted as the most likely explanations for the mechanism of the coaggregation. McGuinness et al (7) hypothesized that heterodimers, which block the formation of dense-cored secretory vesicles, overwhelming the capacity of degradation, can destroy secretory vesicles, leading to aggregation within the cytosol. If this hypothesis is true, wild-type and del32–71 GH should colocalize in secretory vesicles. However, to date, no studies have demonstrated definitive evidence of heterodimers or their colocalization in secretory vesicles. Thus, more detailed evaluations of the interactions between wild-type and del32–71 GH and their subcellular localization are needed.

The third step, a decrease in cell viability, appeared to play a pivotal role in the dominant negative effect in our study. Using GH4C1 cell lines with dox-controlled del32–71 GH expression, we demonstrated that the induction of del32–71 GH decreased wild-type GH secretion and cell viability. The positive correlation between wild-type GH secretion and cell viability suggested that del32–71 GH had a toxic effect on cell physiology. qRT-PCR revealed activation of the 3 major ER stress response pathways, and EM images showed proliferation and enlargement of the ER. The del32–71 GH induction caused DNA fragmentation and activation of caspase-3 and -7, early signs of apoptosis. Finally, overexpression of

XBP1(S) completely reversed the activation of caspase-3 and -7, confirming the causal relationship between del32–71 GH–induced ER stress and apoptosis. Salemi et al (33) demonstrated that del32–71 GH caused reductions in cell proliferation, DNA fragmentation, and apoptosis using fluorescence-activated cell sorting analysis in AtT-20 cell lines. Our data indicate that the effect reported by Salemi et al (33) can be at least partially explained by del32–71 GH–induced ER stress. However, it is still not clear from our study whether ER stress was caused by del32–71 GH alone or by both wild-type and del32–71 GH.

We cannot conclude that ER stress is the sole cause of the dominant negative effect because the T70 cell line demonstrated minimally activated ER stress responses despite the decrease in cell viability and wild-type GH secretion after del32–71 GH induction. Thus, mechanisms other than ER stress must be involved in the dominant negative effect observed in the T70 cell line. However, the involvement of ER stress was definite in the other 4 cell lines in the current study, and thus we consider ER stress to be one of the factors contributing to the dominant negative effect. Our data may complement previous hypotheses such as destruction of secretory vesicles or degradation of aggregated wild-type and del32–71GH.

In our study, the influence of the GHRH signal on the transcription of wild-type and del32–71 GH was not taken into account. Salemi et al (33) and Petkovic et al (21) reported that GHRH stimulation increases del32–71 GH expression preferentially and causes GH deficiency in a vicious cycle. We also note that patients with the *GH1* gene splice site mutations have variable phenotypes, depending on the site of the intronic mutation. The expression of del32–71 GH was shown to increase corresponding with increasing proximity of mutations to the IVS3 splice site (33). We are not able to highlight these various effects because of the use of cDNA constructs. Therefore, we expect that the in vivo dominant negative effect would be much more complex.

Thus, evaluating somatotrophs in vivo using mouse models will give us clues to more thoroughly elucidate the molecular mechanisms mediating the dominant negative effect of del32–71 GH. McGuinness et al (7) established a human del32–71 GH transgenic mouse model and observed severe cellular damage to pituitary cells in this model. Mouse models in which the human wild-type *GH1* gene and human del32–71 *GH1* gene are knocked-in (replacing the mouse *gh1* gene) may be powerful tools in the evaluation of this dominant negative effect and may facilitate the development of new therapeutic interventions, such as overexpression of XBP1(S).

In conclusion, ER stress and apoptosis play a significant role in the dominant negative effect of del32–71 GH resulting from the *GH1* gene splice site mutations. This may explain the evolution of GH deficiency in this disorder. More detailed in vivo studies are necessary in the future.

Acknowledgments

We thank Kazue Kinoshita for assistance with maintenance of cells, Toshimi Michigami for teaching us how to establish stably transfected cell lines, Masahiro Kaburagi for help with measuring wild-type GH concentrations in the culture media by IRMA, Wataru Takahashi and Ryuji Fukuzawa for help with taking EM images, Yasuo Uchiyama and Masaaki Komatsu for advice on the detection of LC3-dependent autophagy activation, Kimi Araki and Ken-ichi Yamamura for providing us antibodies for immunofluorescence studies, and Pinchas Cohen for proofreading of the manuscript.

Address all correspondence and requests for reprints to: Yukihiro Hasegawa, Department of Endocrinology, Tokyo Metropolitan Children's Medical Center, 2–8-29, Musashidai, Fuchu, Tokyo 183–8561, Japan. E-mail: yukihiro_hasegawa@tmhp.jp.

This study was supported by grants from Tokyo Metropolitan Foundation (to Y.H.) and the Foundation of Growth Science in Japan (to D.A.).

Disclosure Summary: The authors have nothing to disclose.

References

1. **Binder G, Ranke MB.** Screening for growth hormone (GH) gene splice-site mutations in sporadic cases with severe isolated GH deficiency using ectopic transcript analysis. *J Clin Endocrinol Metab.* 1995;80:1247–1252.
2. **Cogan JD, Phillips JA, 3rd, Schenkman SS, Milner RD, Sakati N.** Familial growth hormone deficiency: a model of dominant and recessive mutations affecting a monomeric protein. *J Clin Endocrinol Metab.* 1994;79:1261–1265.
3. **Akinci A, Kanaka C, Eble A, Akar N, Vidinlisan S, Mullis PE.** Isolated growth hormone (GH) deficiency type IA associated with a 45-kilobase gene deletion within the human GH gene cluster. *J Clin Endocrinol Metab.* 1992;75:437–441.
4. **Ultsch MH, Somers W, Kossiakoff AA, de Vos AM.** The crystal structure of affinity-matured human growth hormone at 2 A resolution. *J Mol Biol.* 1994;236:286–299.
5. **Graves TK, Patel S, Dannies PS, Hinkle PM.** Misfolded growth hormone causes fragmentation of the Golgi apparatus and disrupts endoplasmic reticulum-to-Golgi traffic. *J Cell Sci.* 2001;114:3685–3694.
6. **Salemi S, Yousefi S, Eble A, Deladoey J, Mullis PE.** Impact of del32–71-GH (exon 3 skipped GH) on intracellular GH distribution, secretion and cell viability: a quantitative confocal microscopy analysis. *Horm Res.* 2006;65:132–141.
7. **McGuinness L, Magoulas C, Sesay AK, et al.** Autosomal dominant growth hormone deficiency disrupts secretory vesicles in vitro and in vivo in transgenic mice. *Endocrinology.* 2003;144:720–731.
8. **Harding HP, Zhang Y, Ron D.** Protein translation and folding are coupled by an endoplasmic-reticulum-resident kinase. *Nature.* 1999;397:271–274.
9. **Haze K, Yoshida H, Yanagi H, Yura T, Mori K.** Mammalian transcription factor ATF6 is synthesized as a transmembrane protein and

activated by proteolysis in response to endoplasmic reticulum stress. *Mol Biol Cell.* 1999;10:3787–3799.
10. **Yoshida H, Haze K, Yanagi H, Yura T, Mori K.** Identification of the cis-acting endoplasmic reticulum stress response element responsible for transcriptional induction of mammalian glucose-regulated proteins: involvement of basic leucine zipper transcription factors. *J Biol Chem.* 1998;273:33741–33749.
11. **Tirasophon W, Welihinda AA, Kaufman RJ.** A stress response pathway from the endoplasmic reticulum to the nucleus requires a novel bifunctional protein kinase/endoribonuclease (Ire1p) in mammalian cells. *Genes Dev.* 1998;12:1812–1824.
12. **Yoshida H.** ER stress and diseases. *FEBS J.* 2007;274:630–658.
13. **Fonseca SG, Fukuma M, Lipson KL, et al.** WFS1 is a novel component of the unfolded protein response and maintains homeostasis of the endoplasmic reticulum in pancreatic beta-cells. *J Biol Chem.* 2005;280:39609–39615.
14. **Imai Y, Soda M, Inoue H, Hattori N, Mizuno Y, Takahashi R.** An unfolded putative transmembrane polypeptide, which can lead to endoplasmic reticulum stress, is a substrate of Parkin. *Cell.* 2001; 105:891–902.
15. **Ito M, Jameson JL, Ito M.** Molecular basis of autosomal dominant neurohypophyseal diabetes insipidus. Cellular toxicity caused by the accumulation of mutant vasopressin precursors within the endoplasmic reticulum. *J Clin Invest.* 1997;99:1897–1905.
16. **Katayama T, Imaizumi K, Honda A, et al.** Disturbed activation of endoplasmic reticulum stress transducers by familial Alzheimer's disease-linked presenilin-1 mutations. *J Biol Chem.* 2001;276: 43446–43454.
17. **Olias G, Richter D, Schmale H.** Heterologous expression of human vasopressin-neurophysin precursors in a pituitary cell line: defective transport of a mutant protein from patients with familial diabetes insipidus. *DNA Cell Biol.* 1996;15:929–935.
18. **Oyadomari S, Koizumi A, Takeda K, et al.** Targeted disruption of the Chop gene delays endoplasmic reticulum stress-mediated diabetes. *J Clin Invest.* 2002;109:525–532.
19. **Sambrook J, Eritsch E, Maniatis T.** *Molecular Cloning: A Laboratory Manual.* New York, NY: Cold Spring Harbor Laboratory Press.
20. **Ishiyama M, Miyazono Y, Sasamoto K, Ohkura Y, Ueno K.** A highly water-soluble disulfonated tetrazolium salt as a chromogenic indicator for NADH as well as cell viability. *Talanta.* 1997;44:1299–1305.
21. **Petkovic V, Godi M, Lochmatter D, et al.** Growth hormone (GH)-releasing hormone increases the expression of the dominant-negative GH isoform in cases of isolated GH deficiency due to GH splice-site mutations. *Endocrinology.* 2010;151:2650–2658.
22. **Kannenberg K, Wittekindt NE, Tippmann S, Wolburg H, Ranke MB, Binder G.** Mutant and misfolded human growth hormone is rapidly degraded through the proteasomal degradation pathway in a cellular model for isolated growth hormone deficiency type II. *J Neuroendocrinol.* 2007;19:882–890.
23. **Ogata M, Hino S, Saito A, et al.** Autophagy is activated for cell survival after endoplasmic reticulum stress. *Mol Cell Biol.* 2006;26: 9220–9231.
24. **Albrecht AN, Kornak U, Boddrich A, et al.** A molecular pathogenesis for transcription factor associated poly-alanine tract expansions. *Hum Mol Genet.* 2004;13:2351–2359.
25. **Ward CL, Omura S, Kopito RR.** Degradation of CFTR by the ubiquitin-proteasome pathway. *Cell.* 1995;83:121–127.
26. **Yoshida H, Matsui T, Yamamoto A, Okada T, Mori K.** XBP1 mRNA is induced by ATF6 and spliced by IRE1 in response to ER stress to produce a highly active transcription factor. *Cell.* 2001; 107:881–891.
27. **Yoshida H, Nadanaka S, Sato R, Mori K.** XBP1 is critical to protect cells from endoplasmic reticulum stress: evidence from site-2 protease-deficient Chinese hamster ovary cells. *Cell Struct Funct.* 2006; 31:117–125.
28. **Schroder M, Kaufman RJ.** Divergent roles of IRE1α and PERK in the unfolded protein response. *Curr Mol Med.* 2006;6:5–36.
29. **Dahmer MK.** Caspases-2, -3, and -7 are involved in thapsigargin-induced apoptosis of SH-SY5Y neuroblastoma cells. *J Neurosci Res.* 2005;80:576–583.
30. **Hayashi Y, Yamamoto M, Ohmori S, Kamijo T, Ogawa M, Seo H.** Inhibition of growth hormone (GH) secretion by a mutant GH-I gene product in neuroendocrine cells containing secretory granules: an implication for isolated GH deficiency inherited in an autosomal dominant manner. *J Clin Endocrinol Metab.* 1999;84:2134–2139.
31. **Iliev DI, Wittekindt NE, Ranke MB, Binder G.** Structural analysis of human growth hormone with respect to the dominant expression of growth hormone (GH) mutations in isolated GH deficiency type II. *Endocrinology.* 2005;146:1411–1417.
32. **Lee MS, Wajnrajch MP, Kim SS, et al.** Autosomal dominant growth hormone (GH) deficiency type II: the Del32–71-GH deletion mutant suppresses secretion of wild-type GH. *Endocrinology.* 2000;141: 883–890.
33. **Salemi S, Yousefi S, Lochmatter D, et al.** Isolated autosomal dominant growth hormone deficiency: stimulating mutant GH-1 gene expression drives GH-1 splice-site selection, cell proliferation, and apoptosis. *Endocrinology.* 2007;148:45–53.
34. **Hamid R, Phillips JA 3rd, Holladay C, et al.** A molecular basis for variation in clinical severity of isolated growth hormone deficiency type II. *J Clin Endocrinol Metab.* 2009;94:4728–4734.

CLINICAL REPORT

AMERICAN JOURNAL OF medical genetics PART A

Delayed Onset Congenital Hypothyroidism in a Patient With *DUOX2* Mutations and Maternal Iodine Excess

Toshihiko Kasahara,[1,2] Satoshi Narumi,[3]* Keisuke Okasora,[2] Ryuzo Takaya,[4] Hiroshi Tamai,[4] and Tomonobu Hasegawa[3]

[1]Department of Pediatrics, Higashitoyonaka Watanabe Hospital, Osaka, Japan

[2]Division of Pediatrics, Hirakata Municipal Hospital, Osaka, Japan

[3]Department of Pediatrics, Keio University School of Medicine, Tokyo, Japan

[4]Department of Pediatrics, Osaka Medical College, Osaka, Japan

Manuscript Received: 12 April 2012; Manuscript Accepted: 17 June 2012

Congenital hypothyroidism (CH), one of the most common congenital endocrine disorders, causes irreversible intellectual disability in untreated patients. Today, the vast majority of patients receive early diagnosis and treatment in the context of newborn screening for CH, and achieve satisfactory cognitive development. However, a subset of patients with delayed onset are undetectable by newborn screening, and miss benefit from early intervention. Here, we report on a delayed-onset CH patient that had two contributing factors in the pathogenesis of CH simultaneously, i.e., a genetic defect and iodine excess. The patient was exposed to excessive iodine in utero because her mother consumed massive amounts of seaweed during pregnancy. Surprisingly, the patient had a negative result in newborn screening, but developed overt CH at age 3 months. She received thyroxine supplementation until when normalization of the thyroid function was confirmed at age 3 years (i.e., transient CH). Mutation screening for *DUOX2*, a causative gene for transient CH, showed biallelic mutations (p.[E327X] + [H678R]). This report provides a new example of environmental modification of phenotypes of CH due to a genetic defect, which can potentially distort screening results.

Key words: congenital hypothyroidism; neonatal screening; false negative reactions; iodine; DUOX2

How to Cite this Article:
Kasahara T, Narumi S, Okasora K, Takaya R, Tamai H, Hasegawa T. 2013. Delayed onset congenital hypothyroidism in a patient with *DUOX2* mutations and maternal iodine excess.
Am J Med Genet Part A 161A:214–217.

INTRODUCTION

Congenital hypothyroidism (CH) is the most common congenital endocrine disorder, affecting about 1 in 3,000 newborns worldwide. In developed countries, majority of patients are detected through newborn screening, in which blood samples on filter paper obtained at age 2–5 days are analyzed. Owing to early diagnosis and treatment, most patients can achieve normal or near normal intellectual outcome today. However, a subset of patients with delayed onset are undetectable by screening, and miss benefit from early intervention.

Inborn errors of thyroid hormone production are collectively referred to as thyroid dyshormonogenesis. Thyroid dyshormonogenesis is a relatively infrequent form of CH, accounting for about 15–20% of cases. Patients with thyroid dyshormonogenesis have a goiter, which results from hyperstimulation of the thyroid by thyroid stimulating hormone (TSH). Genetic defects of a molecule within the thyroid hormone synthesis pathway, such as sodium-iodine symporter (NIS) (*SLC5A5*, OMIM*601843), pendrin (*SLC26A4*, OMIM*605646), dual oxidase 2 (*DUOX2*, OMIM-*606759), thyroid peroxidase (*TPO*, OMIM*606765), and thyroglobulin (*TG*, OMIM*188450), cause thyroid dyshormonogenesis that is inherited as an autosomal recessive trait [Park and Chatterjee, 2005]. These genetic defects account for at least 70% of

Grant sponsor: The Japan Society for the Promotion of Science; Grant sponsor: The Ministry of Health, Labour and Welfare, Japan.
Toshihiko Kasahara and Satoshi Narumi contributed equally to this work.
Conflict of interest: None.
*Correspondence to:
Satoshi Narumi, MD, PhD, Department of Pediatrics, Keio University School of Medicine, Shinanomachi 35, Shinjuku-ku, Tokyo 160-8582, Japan. E-mail: sat_naru@hotmail.com
Article first published online in Wiley Online Library (wileyonlinelibrary.com): 14 December 2012
DOI 10.1002/ajmg.a.35693

thyroid dyshormonogenesis [Narumi et al., 2011], while inappropriate iodine status (i.e., deficiency and excess) can cause transient CH resembling thyroid dyshormonogenesis. In this article, we report a patient with CH due to *DUOX2* mutations, the most common form of thyroid dyshormonogenesis [Narumi et al., 2011], with a delayed onset. Of interest, the patient was compromised by extreme iodine excess during pregnancy, and had a negative result in newborn screening for CH.

CLINICAL REPORT

The patient (a 6-year-old girl) was the first child of healthy nonconsanguineous Japanese parents. Reportedly, the mother of the patient consumed as much as 50–100 g of several kinds of seaweed everyday from the third trimester of pregnancy to 3 months after delivery, in order to "maintain good health". The estimated iodine intake level was 20–40 mg/day, which greatly exceeds the recommended dietary allowance (0.24 mg/day) and tolerable upper intake level (2.2 mg/day) for pregnant women in Japan according to the Dietary Reference Intakes 2010 by Ministry of Health, Labour and Welfare. During the period of seaweed overconsumption, she had neither goiter nor symptoms suggesting hypothyroidism, although we did not test her thyroid function. She did not overconsume seaweeds during the other pregnancy.

The patient was born at 38 weeks with a weight of 2,580 g, and was breastfed. Dried blood samples obtained at age 5 days were subject to newborn screening, in which blood-spot TSH level was measured. The result was negative (screening cutoff TSH level, 10 mU/L). At age 3 months, she had persistent jaundice and poor weight gain (weight, 5,210 g; −2.0 SD). Routine blood tests revealed hyperbilirubinemia (total bilirubin, 6.7 mg/dl) accompanied by a slightly elevated serum aspartate aminotransferase level (105 U/L; ref, 5–45). The thyroid function test showed that she had overt hypothyroidism: TSH, 492 mU/L (ref, 0.3–4.2) and free thyroxine, 0.2 ng/dl (ref, 1.0–1.8). No thyroid autoantibodies were detected. Urinary iodine level was not measured. Thyroid ultrasonography showed a slightly enlarged gland (+1.8 SD [Yasumoto et al., 2004]). Replacement therapy with levothyroxine was initiated, and hyperbilirubinemia and hypertransaminasemia improved subsequently. We reevaluated her thyroid status at age 3 years with discontinuation of therapy. She had normal thyroid function (TSH, 2.3 mU/L; free thyroxine, 1.7 ng/dl), with a normal-sized gland (0.0 SD) on ultrasonography. Thyroidal ^{123}I uptake was normal (24.9% at 24 hr; ref 8–40), with normal perchlorate discharge rate (8.3%; ref <10). The Wechsler Preschool and Primary Scale of Intelligence score evaluated at age 4 years was 93. At last clinical visit, she maintained a normal TSH level without therapy, was growing normally and was developing satisfactory.

Mutation Analysis

DNA samples were collected with written informed consent from the proband, her parents, and her sister. Coding exons and flanking introns of *DUOX2* were analyzed by standard PCR-based sequencing as previously described [Narumi et al., 2011]. The patient was compound heterozygous for a novel nonsense mutation (c.978G>T; c.979G>T, p.E327X) and a known functional single nucleotide polymorphism (c.2033A>G, p.H678R) [Narumi et al., 2011] (Fig. 1A). E327X is a null mutation lacking all functional domains of the DUOX2 protein (Fig. 1A). The DUOX2 allele harboring H678R was shown to have about 60% of residual function in our previous study [Narumi et al., 2011]. The mother and younger sister of the patient were heterozygous for E327X, while the father was heterozygous for H678R (Fig. 1B). These three individuals had normal thyroid function.

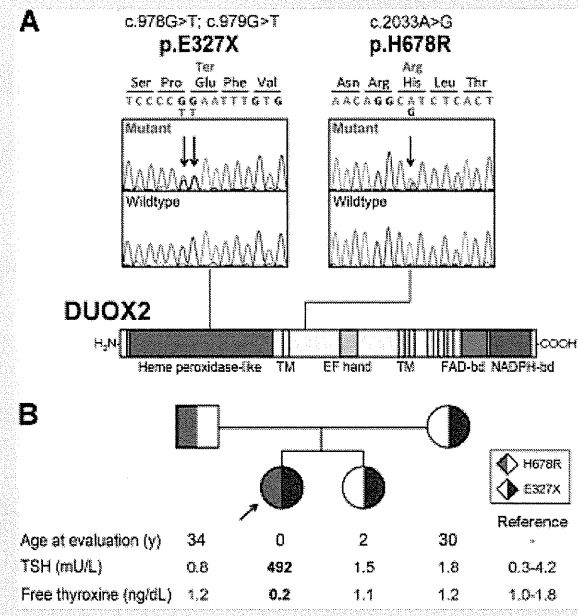

FIG. 1. A: Partial sequences of polymerase chain reaction products of patients are shown along with a schematic diagram of the dual oxidase 2 (DUOX2) protein. Arrows indicate mutated nucleotides. Note that all functional domains of DUOX2 are deleted by the E327X mutation. FAD-bd, flavin adenine dinucleotide binding domain; NADPH-bd, nicotinamide adenine dinucleotide phosphate binding domain; TM, transmembrane segment. B: A pedigree of the patient is shown with clinical parameters, which are aligned with each symbol. Values outside the normal range are typed in boldface.

DISCUSSION

The Japanese consume 1–3 mg of iodine per day [Zava and Zava, 2011], which is one of the highest iodine intake in the world. Perinatal exposure to large amounts of iodine, e.g., maternal ingestion of an iodine-rich drug, is an established cause of transient CH [Theodoropoulos et al., 1979]. The role of milder iodine excess in the pathogenesis of CH remains to be clarified. Nishiyama et al. [2004] studied urine iodine (UI) levels of 34 newborns that were positive at screening for CH in Kumamoto prefecture, Japan, and found that 15 babies had UI levels of greater than 20 μg/dl (a value corresponding to +2 SD of control newborns). Those 15 patients had only slightly high UI level (i.e., mild iodine excess), indicating

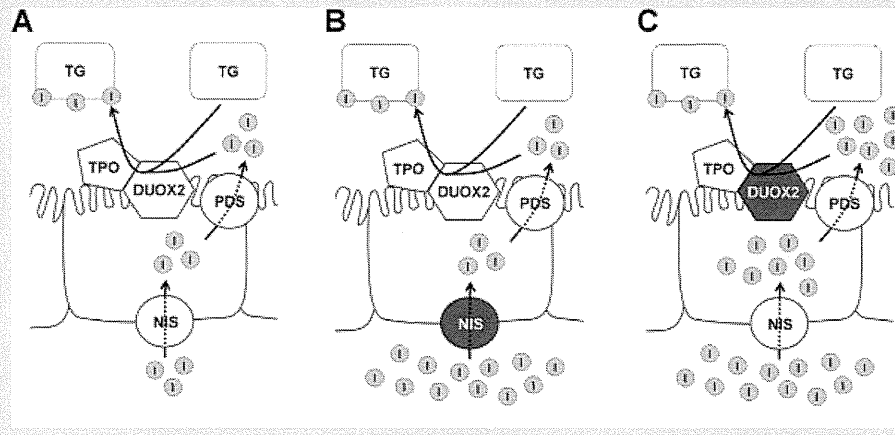

FIG. 2. Schematic diagrams showing a part of the thyroid hormone synthesis pathway. A: Iodine in blood (shown in lower part) is transported into thyroid cells through sodium-iodine symporter (NIS), and then transported into follicular lumen through another transporter named pendrin (PDS). At the apical surface of thyroid cells, iodide is incorporated to thyroglobulin (TG) by thyroid peroxidase (TPO). This reaction requires hydrogen peroxide, which is produced by dual oxidases 2 (DUOX2). B: In a thyroid with the NIS defect, excessive amount of iodine normalizes the defective iodine transportation. C: In a thyroid with the DUOX2 defect, iodine excess presumably compensates the defective iodination of TG.

that mild iodine excess can increase risk of CH. Considering that most newborns with a UI level above +2 SD (constituting 2.3% of population by definition) were assumed to have normal thyroid function, those 15 patients would be affected by other genetic and/or environmental factors making them susceptible to mild iodine excess. In any case, it has been widely accepted that iodine overload in the fetus and newborn negatively affects thyroid function. Therefore, it is notable that thyroid function was not impaired but rather restored by iodine excess in the report of patient with a *DUOX2* defect.

The thyroid hormone-producing capacity varies dramatically in the neonatal period. Several factors influence neonatal TSH and thyroid hormone levels, e.g., TSH surge at birth (followed by transient elevation of thyroid hormone), maturity of hypothalamus-pituitary-thyroid axis, iodine status (deficiency/excess), etc. Timing of onset of TSH rise can be affected by these factors, resulting in negative newborn screen in a subset of patients. Importantly, such false negatives are not rare: A study by Northwest Regional Newborn Screening Program, where second screening at age 2–6 weeks is routinely implemented, showed that the false negative rate of first screening was 7.6% [Hunter et al., 1998]. The public health impact of these false negatives remains to be clarified.

Mechanisms underlying delayed TSH rise are largely unknown except for premature birth. One important model is the genetic defect of NIS, which transports iodine from blood to thyroid cells. The NIS defect, a form of thyroid dyshormonogenesis, has high variability in age at disease onset, ranging from neonatal to adult age [Spitzweg and Morris, 2010]. Of interest, phenotypic expression of the defect is influenced by iodine status: Iodine excess alleviates defective hormone production (Fig. 2) [Matsuda and Kosugi, 1997]. Correspondingly, in our patient with the *DUOX2* mutations, large amount of transplacentally transferred iodine likely prevented her from developing hypothyroidism immediately after birth. A similar mutation-carrying case with a negative screening result has been reported by Vigone et al. [2005], although the level of iodine excess and severity of hypothyroidism differs considerably. The mechanism of alleviation of the *DUOX2* defect by iodine excess is unclear. Considering that thyroid peroxidase and *DUOX2* coordinately incorporate iodine into thyroglobulin at the apical membrane of the thyroid cells, excessive amount of iodine might compensate the defective iodination process (Fig. 2). Alleviation of hypothyroidism by iodine excess has also been reported in a patient carrying mutated dehalogenase 1 [Moreno et al., 2008], the molecule involving in intrathyroidal recycling of iodine. We speculate that similar phenotypic modification could be observed in other forms of thyroid dyshormonogenesis, such as the pendrin defect and the DUOX maturation factor 2 defect.

The main limitation of the present study is the lack of data about urine iodine determination of the proband. In this case, magnitude of iodine excess cannot be discussed in a quantitative manner.

We suspect that not only the NIS defect but also the *DUOX2* defect can have a delayed onset, probably associated with individual iodine status. Because *DUOX2* mutations are the most frequent genetic cause of CH, the defect could be an important source of false negative screen, especially in areas where baseline iodine intake level is high. Future studies targeting screening-negative CH cases will be required to develop more effective screening programs.

REFERENCES

Hunter MK, Mandel SH, Sesser DE, Miyabira RS, Rien L, Skeels MR, LaFranchi SH. 1998. Follow-up of newborns with low thyroxine and nonelevated thyroid-stimulating hormone-screening concentrations: Results of the 20-year experience in the Northwest Regional Newborn Screening Program. J Pediatr 132:70–74.

Matsuda A, Kosugi S. 1997. A homozygous missense mutation of the sodium/iodide symporter gene causing iodide transport defect. J Clin Endocrinol Metab 82:3966–3971.

Moreno JC, Klootwijk W, van Toor H, Pinto G, D'Alessandro M, Leger A, Goudie D, Polak M, Gruters A, Visser TJ. 2008. Mutations in the iodotyrosine deiodinase gene and hypothyroidism. N Engl J Med 358: 1811–1818.

Narumi S, Muroya K, Asakura Y, Aachi M, Hasegawa T. 2011. Molecular basis of thyroid dyshormonogenesis: Genetic screening in population-based Japanese patients. J Clin Endocrinol Metab 96:E1838–E1842.

Nishiyama S, Mikeda T, Okada T, Nakamura K, Kotani T, Hishinuma A. 2004. Transient hypothyroidism or persistent hyperthyrotropinemia in neonates born to mothers with excessive iodine intake. Thyroid 14:1077–1083.

Park SM, Chatterjee VK. 2005. Genetics of congenital hypothyroidism. J Med Genet 42:379–389.

Spitzweg C, Morris JC. 2010. Genetics and phenomics of hypothyroidism and goiter due to NIS mutations. Mol Cell Endocrinol 322:56–63.

Theodoropoulos T, Braverman LE, Vagenakis AG. 1979. Iodide-induced hypothyroidism: A potential hazard during perinatal life. Science 205: 502–503.

Vigone MC, Fugazzola L, Zamproni I, Passoni A, Di Candia S, Chiumello G, Persani L, Weber G. 2005. Persistent mild hypothyroidism associated with novel sequence variants of the DUOX2 gene in two siblings. Hum Mutat 26:395.

Yasumoto M, Inoue H, Ohashi I, Shibuya H, Onishi T. 2004. Simple new technique for sonographic measurement of the thyroid in neonates and small children. J Clin Ultrasound 32:82–85.

Zava TT, Zava DT. 2011. Assessment of Japanese iodine intake based on seaweed consumption in Japan: A literature-based analysis. Thyroid Res 4:14.

Clinical Endocrinology (2013) 78, 957–965 doi: 10.1111/cen.12054

ORIGINAL ARTICLE

A report of two novel *NR5A1* mutation families: possible clinical phenotype of psychiatric symptoms of anxiety and/or depression

Ayuko S. Suwanai*, Tomohiro Ishii*, Hidenori Haruna†, Atsuyuki Yamataka‡, Satoshi Narumi*, Ryuji Fukuzawa§, Tsutomu Ogata¶,** and Tomonobu Hasegawa*

*Department of Pediatrics, Keio University School of Medicine, †Department of Pediatrics and Adolescent Medicine, ‡Department of Pediatric General and Urogenital Surgery, Juntendo University School of Medicine, §Department of Pathology, Tokyo Metropolitan Children's Medical Center, ¶Department of Molecular Endocrinology, National Medical Center for Children and Mothers Research Institute, Tokyo, Japan and **Department of Pediatrics, Hamamatsu University School of Medicine, Shizuoka, Japan

Summary

Objective NR5A1 or steroidogenic factor 1 is a nuclear receptor that plays important roles in the hypothalamus–pituitary–steroidogenic axis. The clinical phenotype of most 46,XY mutation carriers includes disorders of sex development (DSD) without adrenal insufficiency, whereas 46,XX mutation carriers have phenotypes ranging from no symptoms to ovarian insufficiency. Although genetically engineered ventromedial hypothalamus-specific *Nr5a1* knockout mice show anxiety behaviour, no psychiatric symptoms have been reported in human *NR5A1* mutation carriers. We report clinical and molecular findings for individuals (from two families) with *NR5A1* mutations, showing psychiatric symptoms.

Design and methods We screened for *NR5A1* mutations in a cohort of 34 patients with 46,XY DSD using PCR-based sequencing. Psychiatric symptoms were assessed using mental health assessment tools and structured clinical interviews. Functional properties of detected mutant *NR5A1*s were studied *in silico* and *in vitro*, including three-dimensional (3D) mutation models, subcellular NR5A1 protein localization and transactivation assays.

Results We found 2 (46,XY) patients with *NR5A1* heterozygous novel mutations (p.D257fs and p.V424del), which were transmitted from their respective mothers. The patients' clinical findings indicated DSD without adrenal insufficiency. Both mothers showed psychiatric symptoms, including excessive anxiety and/or depression. The mother and grandmother of one patient had premature ovarian insufficiency. Functional studies showed altered 3D models of p.V424del and normal subcellular NR5A1 localization and impaired transcriptional activation without dominant-negative effects in both mutations.

Conclusions We found 2 (46,XX) *NR5A1* mutation carriers with excessive anxiety and/or depression. These results suggest that excessive anxiety and/or depression are possible clinical phenotypes of 46,XX *NR5A1* mutations.

(Received 25 July 2012; returned for revision 9 August 2012; finally revised 28 August 2012; accepted 3 September 2012)

Introduction

NR5A1 (steroidogenic factor 1 [SF1] and AD4BP/FTZF1) is a nuclear receptor expressed in the gonad, adrenal cortex, anterior pituitary, hypothalamus and spleen.[1] NR5A1 plays crucial roles in adrenal and gonadal development, expression of pituitary gonadotrophins and development of the ventromedial hypothalamus (VMH).

Genetically engineered *Nr5a1*-deficient ($Nr5a1^{-/-}$) mice have agenesis of the adrenal glands and gonads, impaired function of pituitary gonadotrophs and VMH abnormalities.[1,2] To define the role of NR5A1 in each tissue, pituitary, VMH and gonadal-specific knockout mice were generated.[2,3]

In humans, the clinical phenotype of most 46,XY mutation carriers is of disorders of sex development (DSD) without adrenal insufficiency. A wide phenotypic spectrum exists in XY DSD subjects, ranging from complete testicular dysgenesis leading to female assignment to severe penoscrotal hypospadias leading to male assignment. The clinical phenotype of 46,XX mutation carriers ranges from no symptoms to ovarian insufficiency.[4] While these gonadal phenotypes have been well described, other phenotypes of *NR5A1* mutations in humans remained unclear. For example, loss of *NR5A1* function in the VMH in humans might cause obesity. Another possibility is anxiety-like behaviour, which has been observed in VMH-specific $Nr5a1^{-/-}$ mice, although no human mutation carrier with psychiatric symptoms has been reported.

Herein, we report two families carrying novel *NR5A1* mutations by screening 34 cases of Japanese 46,XY DSD. We characterized the functional effects of these mutations and evaluated psychiatric symptoms in the affected families.

Correspondence: Tomonobu Hasegawa, Department of Pediatrics, Keio University School of Medicine, 35 Shinanomachi, Shinjuku-ku, Tokyo 160-8582, Japan. Tel.: 81333531211; Fax: 813 53791978; E-mail: thaseg@a6.keio.jp

Patients and methods

Patient report

We enroled 34 Japanese patients with 46,XY DSD with varying degrees of hypospadias (Table 1).

Family 1 (Fig.1a. left). The proband (a 12-year-old female; II-6, Proband 1) was born to nonconsanguineous parents after an uncomplicated pregnancy and delivery (Fig. 1a). Ambiguous genitalia were noticed at birth by obstetricians, and the legal gender was assigned as female. At 9 months of age, clitoromegaly without labial fusion was observed (Fig. 1b). The vaginal and urethral orifices were separated. Small masses were palpable in the labia majora bilaterally. There was no skin hyperpigmentation. Her karyotype was 46,XY. At 13 months of age, the external genitalia showed clitoromegaly (width: 12 mm, length: 15 mm; age-matched Japanese width and length of clitoris; 4·1 ± 1·1 and 4·7 ± 1·1 mm, respectively).[5] Pelvic MRI showed a markedly hypoplastic vagina, and no ovaries or uterus were present. A GnRH stimulation test resulted in LH and FSH peaks of 3·2 and 7·2 U/l, respectively (IFMA, reference value of LH and FSH peak ranges in prepubertal males under 10 years: 1·70–3·77 and 4·38–9·48 U/l, respectively).[6] The basal testosterone concentration was 3·12 nmol/l; after HCG stimulation (3 000 IU/m^2 intramuscularly daily for 3 days), it was increased to 7·32 nmol/l (the basal and stimulated testosterone concentrations following daily injections of 2 000 IU HCG in healthy males aged 5·5–9 years at Tanner stage 1 are 0·62 ± 0·14 and 6·00 ± 0·94 nmol/l, respectively.[7]) Gonadectomy was performed after

Table 1. Phenotypes and genotypes of six subjects with mutations in the *NR5A1* gene

Variable	Family 1			Family 2		
NR5A1 genotype	D257TfsX39 (heterozygous)			V424del (heterozygous)		
	III-6	II-4	I-2	III-4	II-3	III-1
Social sex	Female	Female	Female	Male	Female	Female
Karyotype	46,XY	46,XX	46,XX	46,XY	46,XX	46,XX
Age at last visit (year)	13	40	73	6	46	9
Manifestations	Hypospadia (urogenital sinus) Clitoromegaly Testes in bilateral labia	POI	POI Menopause at 38 years Osteoporosis at 62 years	Hypospadia (penoscrotal) Micropenis Separated scrotum Small testes Enlarged prostatic utricle	Normal	Normal at present
Age at endocrinological examination (year)	1	37		3		
LH/FSH						
Baseline	0·2/0·3	44·1/77·8	ND	<0·1/2·0	ND	ND
GnRH stimulated	3·2/7·2	ND		1·7/18·1		
Basal E2 (nmol/l)	73·4	77·1	ND	29·4	ND	ND
Testosterone(nmol/l)						
Baseline	3·12	<0·05	ND	0·17	ND	ND
HCG stimulated	7·32	ND		1·2		
Psychiatric manifestations	Withdrawn*	Severe depression† Anxiety and depression‡	ND	Anxiety/ Depressed* Aggressive*	Moderate depression†	ND

*Assessed by the Child Behaviour Checklist (CBCL).
†Assessed by the Beck Depression Inventory (BDI)-II.
‡Diagnosed by the Structured Clinical Interview for DSM-IV Axis Disorders (SCID).
POI, premature ovarian insufficiency; ND, not determined, no data; E2, estradiol.
Reference values.
Baseline ranges in boys, aged 1 year: LH, 0·04–0·77 U/l, FSH 0·18–2·06 U/l; aged 3 years: LH, 0·02–0·46 U/l, FSH, 0·2–2·32 U/l as observed using immunofluorometric assay (IFMA) (45).
Stimulated ranges in prepubertal boys, under 10 years: LH, 1·70–3·77, FSH, 4·38–9·48 U/l (IFMA) (12).
Baseline range of after menopause: LH, 11–50, FSH 26–120 U/l, E2 <77·1 nmol/l, progesterone <1·3 nmol/l as observed using electrochemiluminescence immunoassay (ECLIA) (14).
The basal and response testosterone concentrations following daily injections of 2000 IU HCG in healthy boys aged 5·5–9 years at Tanner stage 1; 0·62 ± 0·14 and 6·00 ± 0·94 nmol/l, respectively (14).

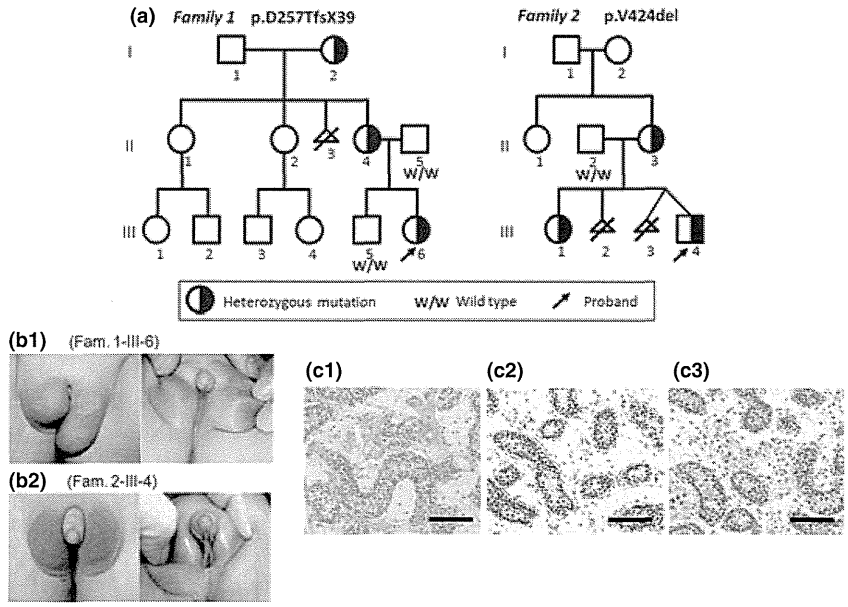

Fig. 1 Pedigrees of two families with 46,XY disorders of sex development and histological analysis of samples from Proband 1. (a) Pedigrees of two families with *NR5A1* mutations. Squares represent male family members and circles represent female family members. Half-solid squares and circles represent carriers of the mutation. Triangles represent miscarriages and deceased twin. The index patient is indicated with an arrow in each family. The genotypes of the parents and siblings of the proband were determined by molecular analysis. (b) Genital features of the probands. Left panel: Proband of Family 1. Right panel: Proband of Family 2. (c. c-1) Gonadal histological analysis (the bar represents 100 μm, H&E) of the Proband 1 shows the small size and decreased numbers of seminiferous tubules (the diameter of the seminiferous tubules: 63·6 μm; age-matched control diameter: 77·4 ± 2·1 μm; the number of the seminiferous tubules was 30–34 tubules/0·64 mm^2; age-matched control: 77·4 ± 2·1 tubules/mm^2) and decreased spermatogonia (the number of spermatogonia per 10 tubular cross-sections is 7–9 and that per 100 Sertoli cells was 3; age-matched control: 13·3 ± 1·3 and 5·9, respectively). The number of Sertoli cells was high (mean, 33 per 10 tubules; age-matched control: 22·2 ± 0·3). Occasionally, foci of aggregated Leydig cells were observed. No Müllerian derivatives could be identified. Gonadoblastoma was not present. (c-2) Immunostaining for wild type (WT)1. Nuclear accumulation of WT1 is restricted to the Sertoli cells. (c-3) Immunostaining for Ad4BP/SF1. Ad4BP/SF1 localized to the nuclei of the Sertoli cells and Leydig cells. The staining intensity of Ad4BP/SF1 varied among the cells.

these stimulation tests. An ACTH stimulation test was normal (data not shown). We initiated oestrogen replacement therapy at 11 years of age. The patient has never had any suspected episodes of adrenal crisis. At present, she attends elementary school as a girl; reportedly, she has had no trouble in her school life.

The mother of the proband (a 38-year-old female; II-4) has normal body proportions and body mass index of 18·8 kg/m^2. Physical examination was unremarkable. Her menarche was at 14 years of age. She became pregnant spontaneously without any fertility treatment and delivered when she was 27 and 28 years old. Her menstrual cycle was regular and 30 days in length (healthy cycle of Japanese women: once per 25–38 days; variation of the interval between menses: <7 days), and the duration of her menstrual bleeding was 2–7 days, although the flow was scanty (duration of healthy menstrual bleeding: 3–7 days; volume: 20–80 ml) until the age of 30 years. Since her early 30s, the duration was less than 2 days. She has always felt anxious, fatigued and unmotivated. She consulted a psychiatrist about these mental health problems, and Clonazepam was prescribed. After she was 36 years old, her menstrual cycles were from 90 to 180 days in length. At 38 years of age, endocrinological assessment showed basal LH 44·1, FSH 77·8 U/l, E2 77·1 nmol/l and progesterone 0·64 nmol/l (ECLIA, reference values after menopause for LH, FSH, E2 and progesterone: 11–50U/l, 26–120 U/l, <77·1 nmol/l and <1·3 nmol/l, respectively).[8] She was diagnosed as having premature ovarian insufficiency by Anasti's criteria,[9] and hormone replacement therapy was initiated. Since the age of 38, she has suffered from irritable bowel syndrome. She has never had a history of obesity or emaciation. She has never had any episode of suspected adrenal crisis.

The maternal grandmother of the proband (I-2) was not obese and entered menopause when she was 38 years old. At the age of 62 years, she was diagnosed with osteoporosis.

Family 2 (Fig.1a. right). The proband (a 6-year-old boy; Fig. 1, III-4, Proband 2) was born to nonconsanguineous parents at full term (Fig. 1a). Ambiguous genitalia was noticed by obstetricians at birth. He had a small penis (stretched penile length of 15 mm; age-matched control length: 27·6 ± 3·6 mm),[10] small testes (volumes less than 1 ml, in the scrotum; age-matched control volumes: 1–2 ml),[11] penoscrotal hypospadias, bifid scrotum and an enlarged prostatic utricle that opened below the urethral meatus (Fig. 1b). No skin hyperpigmentation was observed. The karyotype was 46,XY, and the patient was raised as a boy. At 3 years of age, a GnRH stimulation test showed LH

and FSH peaks of 1·7 and 18·1 U/l. The basal testosterone concentration was 0·17 nmol/l and, after stimulation, increased to 1·2 nmol/l. ACTH stimulation test was normal (data not shown). At 3 years of age, urethroplasty was performed. No adrenal crisis occurred during surgery.

The mother of the proband (a 46-year-old woman; II-3) had an unremarkable medical history and physical examination. She developed menarche at 13 years of age. She gave birth spontaneously when she was 32 and 40 years old. Her menstrual cycle was regular and 30 days, although the duration of menstrual bleeding reduced after the age of 35. When she was 40 years old, her menstrual cycles ranged from 15 to 60 days, and the flow was scanty. She complained of fatigability, listlessness and lack of concentration. No endocrinological examination was performed. She does not have a history of obesity or emaciation. She has never had any episodes of suspected adrenal crisis. The sister of the proband (III-2) was clinically normal and her menarche was at the age of 13 years.

Intelligence quotient (IQ), mental state and behavioural assessment

Intelligence quotients (IQs) were evaluated using the Wechsler Intelligence Scale for Children-III . Problem behaviours in the children were evaluated by the Child Behaviour Checklist (CBCL).[12] The Beck Depression Inventory (BDI)-II[13] was used to screen depression in the mothers of Probands 1 and 2. The following cut-offs were used for depression: 0–13 points, minimal; 14–19, mild; 20–28, moderate; 29–63, severe. The Structured Clinical Interview for Diagnostic and Statistical Manual of Mental Disorders IV (DSM-IV) Axis Disorders (SCID) was performed on the mother of Proband 1.

Gonadal histology

Haematoxylin and eosin-stained standard sections from Proband 1 were evaluated. Four-micrometre sections of formalin-fixed, paraffin-embedded tissue specimens were used for immunostaining. Antigen retrieval was performed by boiling in citrate buffer. NR5A1 was used as a primary antibody,[14] and the simple stain MAX-PO system (Nichirei, Tokyo, Japan) was used to detect the primary antibody. For comparison, testes from three foetus obtained at autopsy at the 23th–30th weeks of gestation were examined for NR5A1 expression.

Mutational analysis

We obtained written informed consent from the patients or parents. The study was approved by the institutional review board. We extracted genomic DNA from peripheral blood. The entire coding regions of *NR5A1* were amplified by PCR (the primer sequences are available on request) and sequenced using Big Dye Dideoxy Sequence Kit (Applied Biosystems, Foster City, CA, USA) and an ABI3130xl automated sequencer (Applied Biosystems). Detected mutations were tested in 60 Japanese healthy controls.

Three-dimensional (3D) models of NR5A1 proteins

The three-dimensional (3D) models of the ligand-binding domain (LBD) of both wild type (WT) and p.V424-deleted NR5A1 proteins were created using the 3D-JIGSAW web-based interface. Images of the modelled proteins (schematic) were viewed and manipulated using Deep View (The Swiss Institute of Bioinformatics).[15]

Construction of expression vectors

We generated N-terminal enhanced green fluorescent protein (EGFP)-tagged NR5A1 by cloning the PCR-amplified WT *NR5A1* cDNA in-frame into a pEGFP-C1 (CLONTECH, Palo Alto, CA, USA) via introduced restriction sites (*Eco*R1/*Bam*H1). We created untagged *NR5A1* vectors by removing GFP from the pEGFP-C1-NR5A1 vectors. Three mutants (D257TfsX39, V424del, and L442X) were generated by site-directed mutagenesis (QuikChange IIXL; Stratagene, La Jolla, CA, USA). L442X has a stop codon immediately before the activation function domain 2 (AF2). The luciferase reporter constructs CYP11A1 and CYP19A1 have been described previously.[16,17]

Cell culture and transfection

We cultured HEK293 cells for luciferase assays and western blots, and COS-7 cells for the GFP study. We transfected WT or mutant plasmids to each cell using Lipofectamine™ 2000 reagent (Invitrogen, Carlsbad, CA, USA) according to the manufacturer's protocol.

Visualization of subcellular localization

COS-7 cells grown on sterile glass coverslips were transfected with WT or mutant pEGFP-tagged *NR5A1* (0·8 mg). Twenty four hours after transfection, cells were fixed in 2% formaldehyde/PBS. The cover slips were subsequently mounted with Vectashield mounting medium with 4′,6-diamidino-2-phenylindole (DAPI; Vector Laboratories, Burlingame, CA, USA) and were observed under a BX-50 fluorescence microscope (Olympus, Tokyo, Japan).

Transactivation assay

Untagged-*NR5A1* WT or mutant expression vectors (150 ng/well with CYP11A1 reporter or 30 ng/well with CYP19A1 reporter) were transfected into HEK293 cells with reporters (200 ng/well). The WT and mutant (1:1) were cotransfected with the reporters to determine possible dominant-negative effects. Twenty four hours after transfection, cells were analysed using the Dual Luciferase Reporter assay system (Promega, Madison, WI, USA) according to the manufacturer's protocol. Each result is representative of three independent experiments that yielded similar results. The results are expressed as mean ± standard error of the mean (SEM), and statistical significance was determined by *t*-test.

Western blotting

We extracted the proteins from whole HEK293 cells, which were transfected with a vector containing either WT or mutant *NR5A1*. Extracted proteins were analysed by SDS-PAGE and Western blotting. We used the primary and secondary antibodies described before.[14]

Results

IQ, mental state and behavioural assessment

Family 1. The proband (II-6) was assessed at 11 years of age. Her full-scale IQ was 114. Her CBCL score was in the borderline clinical range on the 'Withdrawn' domain (Table 1).

The mother of the proband (II-4) scored 40 and 35 (at 38 and 40 years of age) on the BDI–II, indicating severe depression. She was diagnosed with depressive disorder and generalized anxiety disorder by the SCID. She had seven of the nine symptoms in the diagnostic criteria for a major depressive episode. She also mentioned that she had been having excessive anxiety, vague unpleasant emotions and difficulty in controlling her anxiety since childhood.

Family 2. The proband (III-5) was assessed with the CBCL at 6 years of age. His scores on the 'Anxious/Depressed' and 'Aggressive Behaviour' domains were in the clinical range. His score on the 'Attention Problems' and 'Rule-Breaking Behaviour' scales were in the borderline clinical range.

The mother of the proband (II-3) scored 23 on the BDI-II at 46 years of age, indicating moderate depression.

Histopathology

Samples from Proband 1 obtained at 13 months of age were taken for pathological analysis. Grossly, the gonads were hypoplastic and measured 0·9 × 0·8 cm (on the right) and 1·2 × 0·7 cm (on the left). Histologically, both had similar features (Fig. 1c-1). Müllerian duct-derived tissues were not present. Seminiferous tubules had lost their back-to-back structures and were present in the stroma. The lumen of the seminiferous tubules was primarily composed of Sertoli cells with a minority of spermatogonia as highlighted by nuclear WT1 immunostaining (Fig. 1c-2). Unexpectedly, multiple foci of aggregated foamy probable Leydig cells were noted around the seminiferous tubules. Positive nuclear NR5A1 immunostaining confirmed that these foamy cells were Leydig cells (Fig. 1c-3). From the nuclear accumulation of NR5A1 and the absence of cytoplasmic granular staining patterns, the immunostaining pattern of the NR5A1 protein in the Leydig cells of this patient was found to be similar to that observed in the 3 male foetuses.

Mutational analysis

Mutational analysis of the *NR5A1* gene revealed a heterozygous frameshift mutation, c.768del, D257TfsX39 (Fig. 2) in Proband 1. This mutation was transmitted from her mother and grandmother. This mutation is predicted to alter the protein sequence and create a premature termination codon at codon 296. A heterozygous c.1268_1270delTGG, p.V424del mutation (Fig. 2) was detected in Proband 2. This mutation was transmitted from his mother to Proband 2 and his sister. These two mutations were not observed in the 120 alleles of adult controls.

3D models of NR5A1 proteins

Our model of V424del indicated a change in the loop's shape (Fig. 3, Panels b and c) and the angle of Helix 11 compared with those of WT (Panels d and e). The amino acids in an alpha helix are arranged in a right-handed helical structure in which each amino acid residue corresponds to a 100° turn in the helix and a translation of 0·15 nm along the helical axis. Therefore, the change in the angle of the N-terminal end of Helix 11 was approximately 100°.

Visualization of subcellular localization of NR5A1 proteins

The WT and both mutant proteins were exclusively localized in the nucleus (Fig. 4).

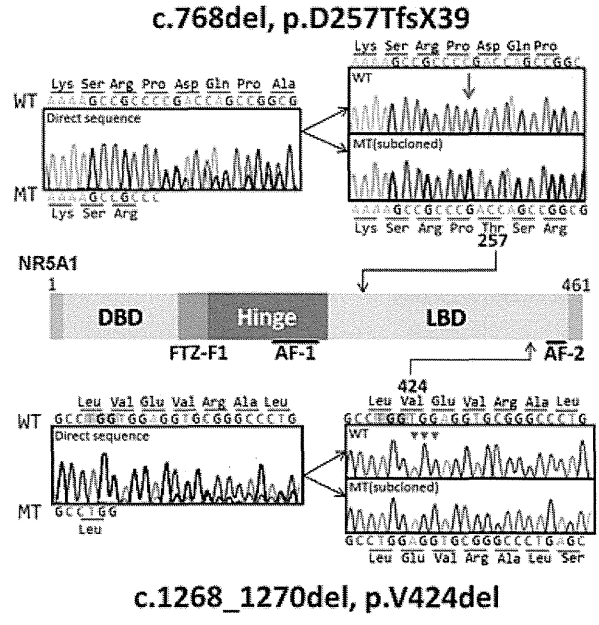

Fig. 2 Detection of mutations. The functional domains of the NR5A1 protein are shown, including the two mutations described in this study. Representative chromatograms are shown for each mutation. Each mutation was subcloned. The DNA-binding domain (DBD) containing two zinc-finger motifs is indicated. The FtzF1 box stabilizes protein binding to DNA. The hinge region is important for stabilizing the ligand-binding domain (LBD) and interacts with other proteins that control NR5A1 transcriptional activity. The activation function 2 (AF2) domain recruits cofactors necessary for NR5A1 transactivating activity.

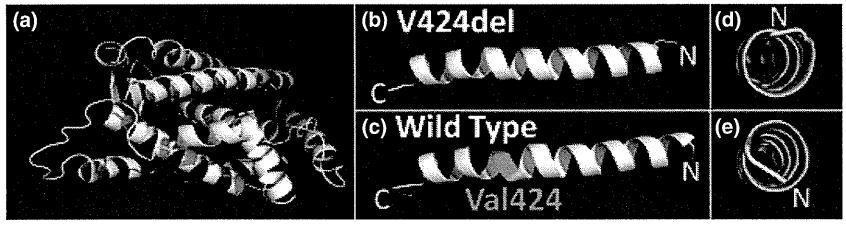

Fig. 3 3D models of wild type (WT) and mutated NR5A1 proteins. 3D models of the whole LBD (CYS407-GLY442) (a) and Helices 10 and 11 of the LBD of the WT (b) and V424del-mutated NR5A1 proteins (c) were obtained with the use of the 3D-JIGSAW web-based interface. Val 424 in the WT protein is shown in pink, and the N-terminal side end of Helix 11 is shown in yellow. Note the change of the angle of N-terminal end of Helix 11 (d and e) indicating the shift of the position of the AF2 domain in Helix 12 (red arrow in a).

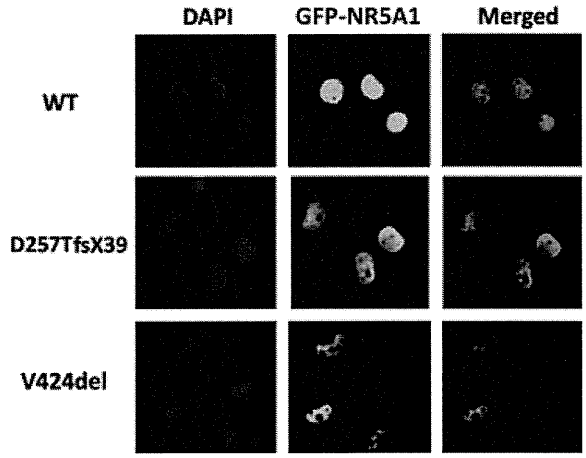

Fig. 4 Cellular localization of NR5A1 mutants. Cellular localization of GFP-NR5A1 fusion proteins (green) generated and expressed in COS-7 cells with the use of a pEGFP-C1 vector. Wild type (WT) NR5A1 showed nuclear localization. Expression and localization patterns similar to that of the WT are seen for the V424del and the D257fs mutants.

Transactivation assay

The analysis of WT and mutant NR5A1 functions showed impaired activity for the three mutants (D257fs, V424del and L442X) on NR5A1 target gene promoters (Fig. 5). D257fs showed residual transactivation activity of WT NR5A1 (CYP11A1: 60·0 ± 0·12; CYP19A1: 23·9 ± 2·3). V424del markedly impaired activities, which were the same as that observed for the empty vector in both promoters. L442X had the same activity as that observed for the empty vector in both CYP11A1 and CYP19A (data not shown). Cotransfection of the mutants (D257fs or V424del) in a 1:1 ratio with WT *NR5A1* did not impair the transactivation capacity of the WT protein, indicating that no dominant-negative effect occurred.

Western blot analysis

The WT-NR5A1 protein and the V424del protein were detected as the same size bands. The D257fs protein was not detected (data not shown).

Discussion

We sequenced *NR5A1* in a cohort of 46,XY DSD patients with varying degrees of hypospadia and found 2 unrelated families with a novel heterozygous *NR5A1* mutation. Two 46,XY mutation carriers showed severe submasculinization. Each mutation was transmitted from mothers. Two 46,XX mutation carriers showed premature ovarian insufficiency. Notably, we investigated *NR5A1* mutation carriers' mental status for the first time and found one 46,XX mutation carrier who was depressed and had anxiety disorder and another who was depressed.

We confirmed that two novel *NR5A1* mutations (D257fs and V424del) caused losses of function, without dominant-negative effects, thus resulting in haploinsufficiency. The D257fs (c.768del) mutation, which lacked approximately 85% of the LBD, had some residual activity *in vitro*. D257 is located at exon 4, which is not the last exon, and D257fs has a stop codon that is located downstream of 39 extra amino acids. Thus, the D257fs transcript is likely to be degraded by nonsense-mediated decay, leading to haploinsufficiency *in vivo*. V424del (c.1268_1270delTGG) was predicted to result in the deletion of an amino acid in the LBD of NR5A1. V424del is highly conserved and is located in Helix 11 of the LBD. The change in the angle of Helix 11 indicated by our 3D model was predicted to dramatically alter NR5A1 activity, consistent with the failure of mutant NR5A1 to transactivate promoters.

Our findings suggested that *NR5A1* mutations resulted in psychiatric symptoms in 46,XX patients. Indeed, among 4 (46,XX) mutation carriers, two showed psychiatric symptoms; anxiety and depression were present in the mother of Proband 1, and there was depression in the mother of Proband 2. The results of the BDI-II indicated that both mothers had moderate to severe depression. The mother of Proband 1 was further diagnosed with major depression and general anxiety disorder by the SCID. Unfortunately, it is uncertain whether the mother of Proband 2 had anxiety, because she refused further mental assessment. The grandmother of Proband 1 and the sister of Proband 2 also declined to undergo any psychological assessment. Some important issues should be discussed regarding psychiatric symptoms. Firstly, we speculate that psychiatric symptoms in 46,XX individuals are due to decreased expression of *NR5A1* target genes in VMH, judging from the phenotypes of VMH-specific *Nr5a1*$^{-/-}$ mice, showing increased anxiety behaviour compared with their

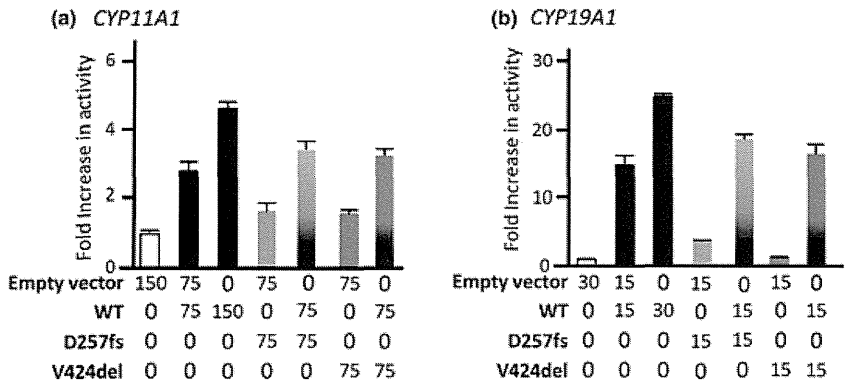

Fig. 5 Assays of NR5A1 transcriptional activity. The transcriptional activities of wild type (WT) NR5A1 (black bar) and the mutants (blue and red bar) were studied with the use of CYP11A1 (a) and CYP19A1 (b) promoters in HEK293 cells. Results are expressed as fold activity over empty vector (white bar). The under numbers show the concentrations (in ng) of the vectors. D257fs resulted in loss of function (WT: D257fs, CYP11A1, $P < 0{\cdot}05$ and CYP19A, $P < 0{\cdot}002$), no dominant-negative effect (WT1 allele: WT+D257fs, CYP11A1, $P > 0{\cdot}12$ and CYP19A, $P > 0{\cdot}07$) and haploinsufficiency (WT2 alleles: WT+D257fs, CYP11A1, $P < 0{\cdot}02$ and CYP19A, $P < 0{\cdot}001$). V424del showed loss of function (WT: V424del, CYP11A1 $P < 0{\cdot}02$ and CYP19A, $P < 0{\cdot}005$), no dominant-negative effect (WT1 allele: WT+V424del, CYP11A1, $P > 0{\cdot}16$ and CYP19A, $P > 0{\cdot}29$) and haploinsufficiency (WT2 alleles: WT+V424del, CYP11A1, $P < 0{\cdot}01$ and CYP19A $P < 0{\cdot}002$). Data represent the mean of 3 independent experiments, each performed in triplicate. The T-bars represent the standard error of the mean (SEM). Cotransfection of mutants with WT NR5A1 did not show a dominant-negative effect.

WT counterparts.[18] As the knockout mouse mutation is homozygous and all *Nr5a1* regulated functions are lost in VMH, whereas human mutations are heterozygous, psychiatric symptoms in mice might not be seen in all human patients. Possible target genes in the VMH are brain-derived neurotrophic factor (*BDNF*) and corticotrophin-releasing hormone receptor 2 (*CRHR2*), as these genes are related to stress and anxiety.[19] Secondly, psychiatric symptoms have not been reported in any 46, XX mutation carriers in the literature. To our knowledge, more than 20 (46,XX) mutation carriers, including five children have been reported to date.[4,20–28] These patients were probably not evaluated psychiatrically. Alternatively, psychiatric symptoms might become more apparent with age. Third, in 46,XX adult carriers, psychiatric status may be related to having a DSD child and suffering from POI. In our study, the mother of Proband 1 showed separation anxiety during childhood, indicating that some of her psychiatric symptoms must have existed before having a DSD child or suffering from POI. Fourth, in 46,XY mutation adult and child carriers, exploring whether *NR5A1* mutations cause psychiatric symptoms is difficult. Carriers of 46, XY mutations have DSD or azoospermia, which highly affects psychiatric status as observed in patients with other DSDs.[29] We cannot dissect their pathogenesis that is a direct effect of *NR5A1* mutations *vs* the psychiatric effects of adaptation to DSD or azoospermia, although the two probands in our study had some problems in their behaviour as indicated by the CBCL. Moreover, there may be sexual dimorphism in psychiatric symptoms associated with NR5A1, similar to the higher prevalence of depression and anxiety among females in the general population. Fifth, the possibility that these mothers' psychiatric symptoms could simply represent the incidence in the general population and/or simply be the result of family and personal problems cannot be completely ruled out.

The phenotypes of our 46,XY probands (hypospadias without adrenal insufficiency) were consistent with previous reports. In 2009, Kohler *et al.*[30] found three *NR5A1* mutations in 60 patients with hypospadias. In 2011, Allali *et al.* reported one of 33 patients with hypospadias.[28] Taken together, *NR5A1* mutation carriers were found in approximately 5% (6/127) of hypospadias cases.

We confirmed that in females, *NR5A1* heterozygous mutations are associated with premature ovarian insufficiency without adrenal insufficiency. We found four (46,XX) mutation carriers through family analysis, of whom two (the mother and grandmother of Proband 1) had premature ovarian insufficiency. The mother of Proband 2 had seemingly normal ovarian function. The long-term ovarian function of the sister of Proband 2 is not yet clear although her breasts developed normally and her menarche began spontaneously.

We found abundant Leydig cells in the testes of a 13-month-old patient. In previous reports, clusters of Leydig cells were observed in four cases of *NR5A1* mutations in patients aged from 6 months to 2 years,[21,23,26] similar to our observation. Normally, Leydig cells are not recognized after mini-puberty until immediately before puberty. Leydig cells before mini-puberty are called foetal Leydig cells (FLCs), and those after puberty are adult Leydig cells (ALCs).[31,32] We assume that the abundant Leydig cells found in our patient are FLCs because of the age of the patient and the immunostaining pattern; the patient was 13 months old, and ALCs are rarely observed at this age. Recently, Cools *et al.*[33] reported Leydig cell hyperplasia in a pubertal 13-year-old mutation carrier. They showed a homogenous NR5A1 staining pattern in the nuclei and a granular staining pattern in the cytoplasm of ALCs in the carrier and a normal adult, while this pattern was observed in the nuclei of FLCs in a normal foetus. The immunostaining pattern in our